A R C H I V E S O F M E T A L L U R G Y A N D M A T E R I A L S
Volume 57 2012 Issue 1
DOI: 10.2478/v10172-011-0159-9

W. WOŁCZYŃSKI*, E. GUZIK**, W. WAJDA*, D. JĘDRZEJCZYK***, B. KANIA*, M. KOSTRZEWA****

CET IN SOLIDIFYING ROLL – THERMAL GRADIENT FIELD ANALYSIS

KRT W KRYSTALIZUJĄCYM WALCU – ANALIZA GRADIENTOWEGO POLA TEMPERATURY

As the first step of simulation, a temperature field for solidifying cast steel and cast iron roll was created. The convection in the liquid is not comprised since in the first approximation, the convection does not influence the analyzed occurrence of the $C \rightarrow E$ (columnar to equiaxed grains) transition (CET) in the roll. The obtained temperature field allows to study the dynamics of its behaviour observed in the middle of the mould thickness. This midpoint of the mould thickness was treated as an operating point for the $C \rightarrow E$ transition. A full accumulation of the heat in the mould was postulated for the $C \rightarrow E$ transition. Thus, a plateau at the $T(t)$ curve was observed at the midpoint. The range of the plateau existence $t_C \leftrightarrow t_E$ corresponded to the real period of transition, $t_C^R \leftrightarrow t_E^R$ that occurs in the solidifying roll.

At the second step of simulation, the thermal gradients field was studied. Three ranges were distinguished:

a/ for the formation of the columnar structure (the C – zone):

$\left(\dot{T} \gg 0 \text{ and } \left(G\Big|_{t<t_C^R} - G\Big|_{t=t_C^R}\right) \gg 0\right)$,

b/ for the $C \rightarrow E$ transition (from columnar to fully equiaxed structure):

$\left(\dot{T} \approx 0 \text{ and } \left(G\Big|_{t=t_C^R} - G\Big|_{t=t_E^R}\right) \approx 0\right)$,

c/ for the formation of the fully equiaxed structure (the E – zone):

$\left(\dot{T} < 0 \text{ and } \left(G\Big|_{t=t_E^R} - G\Big|_{t>t_E^R}\right) \approx 0\right)$.

The columnar structure formation was significantly slowed down during incubation period. It resulted from a competition between columnar growth and equiaxed growth expected at that period of time. The $\left(G\Big|_{t=t_C^R} - G\Big|_{t=t_E^R}\right) \approx 0\right)$ relationship was postulated to correspond well with the critical thermal gradient, $G_{crit.}$.

A simulation was performed for the cast steel and cast iron rolls solidifying as if in industrial condition. Since the incubation divides the roll into two zones (columnar and equiaxed) some experiments dealing with solidification were made on semi-industrial scale.

A macrosegregation equation for both mentioned zones was formulated. It was based on a recent equation for redistribution after back-diffusion. The role of the back-diffusion parameter was emphasized as a factor responsible for the redistribution in columnar structure and equiaxed structure.

Keywords: solidifying roll, thermal gradient field, columnar into equiaxed structure transition, macro-segregation index

W pierwszym etapie symulacji wygenerowano numerycznie pole temperatury dla krzepnącego walca staliwnego oraz żeliwnego. Nie uwzględniono konwekcji uznając, że w pierwszym przybliżeniu konwekcja nie wpływa na przebieg transformacji $C \rightarrow E$ (struktura kolumnowa w równoosiową, CET). Uzyskane pole temperatury pozwala na analizę jego zachowania w środku grubości wlewnicy. Ten punkt wlewnicy zostałpotraktowany jako punkt operacyjny dla transformacji $C \rightarrow E$. Postuluje się w tym modelu, że zachodzi pełna akumulacja ciepła we wlewnicy właśnie dla tej transformacji. Stąd, spłaszczenie krzywej $T(t)$ jest obserwowane dla punktu operacyjnego. Zakres tego spłaszczenia oznaczony $t_C \leftrightarrow t_E$ odpowiada rzeczywistemu okresowi transformacji, $t_C^R \leftrightarrow t_E^R$ który pojawia się w krzepnącym walcu.

W drugim etapie symulacji analizuje się gradientowe pole temperatury. Wyróżniono trzy jego zakresy:

a/ dla formowania się struktury kolumnowej (strefa C):

$\left(\dot{T} \gg 0 \text{ oraz } \left(G\Big|_{t<t_C^R} - G\Big|_{t=t_C^R}\right) \gg 0\right)$,

b/ dla transformacji struktury kolumnowej w strukturę w pełni równoosiową (okres inkubacji), $C \rightarrow E$:

* INSTITUTE OF METALLURGY AND MATERIALS SCIENCE, POLISH ACADEMY OF SCIENCES, 30-059 KRAKÓW, 25 REYMONTA STR., POLAND
** AGH – UNIVERSITY OF SCIENCE AND TECHNOLOGY, FACULTY OF FOUNDRY ENGINEERING, 30-059 KRAKÓW, 25 REYMONTA STR., POLAND
*** UNIVERSITY OF BIELSKO-BIAŁA, 43-309 BIELSKO-BIAŁA, 2 WILLOWA STR., POLAND
**** ECO-HARPOON, ECOLOGICAL TECHNOLOGIES COMPANY LTD, 05-152 CZOSNÓW, CZĄSTKÓW MAZOWIECKI 152, POLAND

$\left(\dot{T} \approx 0 \text{ oraz } \left(G\Big|_{t=t_C^R} - G\Big|_{t=t_E^R}\right) \approx 0\right)$,
c/ dla formowania się struktury równoosiowej (strefa E):
$\left(\dot{T} < 0 \text{ and } \left(G\Big|_{t=t_E^R} - G\Big|_{t>t_E^R}\right) \approx 0\right)$.

Powstawanie struktury kolumnowej wyraźnie zwalania w okresie inkubacji. Wynika to z konkurencji między wzrostem struktury kolumnowej i równoosiowej. Postuluje się że zaobserwowana zależność $\left(G\Big|_{t=t_C^R} - G\Big|_{t=t_E^R}\right) \approx 0\right)$ dobrze odpowiada krytycznemu gradientowi temperatury, $G_{crit.}$.

Symulacja została przeprowadzona zarówno dla walców staliwnych jak i żeliwnych dla warunków zbliżonych do przemysłowych. Ponieważ tzw. inkubacja dzieli walec na dwie strefy (kolumnową i równoosiową) pewne eksperymenty związane z symulacją zostały przeprowadzone w skali półprzemysłowej celem konfrontacji z obliczeniami.

Sformułowano równanie określające makrosegregację w obu strefach. Bazuje ono na ostatnio zaproponowanym równaniu dla opisu redystrybucji po dyfuzji wstecznej. Podkreślono rolę parametru dyfuzji wstecznej jako czynnika odpowiedzialnego za redystrybucję w obu strefach strukturalnych.

1. Introduction

Rolls made of steel, cast steel and cast iron are expensive tools which have to meet very high requirements. The rolls should be resistant to abrasive wear, to mechanical and thermal fatigues and to crack propagation. Thus, the chemical composition of rolls are imposed by the mandatory standards.

However, some companies offer rolls with various combinations of the elements, such as: C, Si, Cr, Ni, Mo.

The $C \leftrightarrow E$ transition (CET) in solidifying rolls was already discussed to a large degree, [1]. The solid / liquid interface undercooling for both structures formation was the subject of this description. The estimated values of temperature gradient were based on this undercooling, [1]. By the use of the mentioned theory, [1] it was possible to localize the $C \leftrightarrow E$ transition through analysis of the difference between velocities of the *liquidus* isotherm and *solidus* isotherm.

The size of columnar and equiaxed grains was compared in order to verify theoretical predictions, [2].

As far as undercooling calculations are concerned, they are to some extent uncertain.

They concern the solid/liquid interface and are not associated with the solidification taken as a whole.

The $C \leftrightarrow E$ transition was simulated numerically by means of the SOLID Software, [3], The simulation requires some data from the experiment, which are difficult to obtain, particularly in the industrial conditions. The transition from constrained to unconstrained growth was also studied, but during directional solidification only, [4]. The model was based on the phenomenon of destabilization in order to confront the results of theoretical simulation with experimental observations.

The mentioned calculations [4], did not include the field of the thermal gradients. The thermal gradients, both in the liquid at the dendrite/cell tips and in the mushy zone, were determined in a different way.

The current work makes an attempt to find a correlation between thermal gradients field and a $C \leftrightarrow E$ transition in the roll in order to optimize the roll structure and its properties in the future.

Thus, the current work presents a new mode of description of the $C \leftrightarrow E$ transition by calculating the gradients field for the real temperature and by treating the incubation period as the most significant phenomenon that appears during solidification (particularly for the $C \leftrightarrow E$ transition).

The calculations were performed on the computer located at the Academic Computer Centre CYFRONET – AGH Kraków, (computer named "BARIBAL", financed by the research project MNiSW/SGI3700/PAN/021/2009).

The details of the calculation method are described in the manual, [5].

NOMENCLATURE

f	–	heat flux, Eq. (2),
G	–	thermal gradient, $G = \partial T/\partial r\,\big|_{liquidus}$,
$\overline{H}$	–	total height of a frozen columnar grain, Fig. 22,
h	–	heat transfer coefficient,
$i_{macr.}$	–	macrosegregation index within a given area of roll,
k	–	partition ratio,
$\overline{L}$	–	half the size of a frozen grain and precipitate, Fig. 22,

$\overline{L}_0$ – half the size of frozen columnar grain referred to a given height of the columnar grain, Fig. 22,
$\overline{L}_{0i}$ – half the size of a frozen columnar grain referred to current heights of the columnar grain for the i-th point imposed by the EDAX measurement, Fig. 22,
N_B – solute redistribution after back-diffusion, Eq. (3),
$\overline{N}_i^{\beta}$ – solute redistribution measured at the i-th point, Fig. 23,
$N_B^{\max}$ – maximal solute redistribution within an area, Eq. (3),
$N_B^{\min}$ – minimal solute redistribution within an area, Eq. (3),
N_L – solute concentration in the liquid, Eq.(3),
N_0 – nominal solute concentration in a given alloy,
q – heat flux per unit area of the body, Eq. (1),
R – equiaxed grain radius, (representative grain), Fig. 23,
$\overline{R}$ – radius of a given equiaxed grain, Fig. 23,
$\overline{R}_d$ – radius of the spherical cap, Fig. 23,
r – roll radius,
$r_{liq.}$ – *liquidus* temperature position,
S – surface area, Eq. (1),
T – temperature,
T_g – temperature at the roll/mould border, Figs 6-9,
T_{liq} – *liquidus* temperature,
t – time,
t_C – time, when the operating point reveals vanishing of the columnar structure formation, Fig. 3,
t_E – time, when the operating point reveals the fully equiaxed structure formation, Fig. 3,
t_C^R – time, when columnar structure vanishes in the roll and competition between columnar structure and equiaxed structure formation appears, Figs 10, 14,
t_E^R – time, when competition between columnar and equiaxed structure growth is completed and fully equiaxed structure formation is expected, Figs 10, 14,
U – internal energy of the liquid/solid system, Eq. (1),
V – volume of the solid, Eq. (1),
v – rate of the *liquidus* isotherm movement,
v_C – rate of the columnar structure growth,
x – current amount of a growing grain,
x_i – current amount of a growing columnar grain for i-th point imposed by the EDAX measurement of solute redistribution within a given columnar grain, Fig. 22,
x^0 – amount of a given grain (primary phase) at which process was stopped and morphology frozen, Fig. 22,
x_{0i} – amount of a given grain at which solidification was arrested for i-th point imposed by the EDAX measurement of solute redistribution, Fig. 22,
z – position, Eq. (2),
α – back-diffusion parameter, Eq. (3),
β^{ex} – coefficient of the extent of redistribution, Eq. (3),
β^{in} – coefficient of the intensity of redistribution, Eq. (3),
λ – thermal conductivity matrix, Eq. (2),
$\overline{\lambda}_i$ – current distance for the i-th point imposed by the EDAX measurement of solute redistribution, Fig. 22,

θ^0 – external temperature, Fig. 1,
ρ – density, Eq. (1),
σ – heat supplied externally into body, Eq. (1).

2. Method of temperature field calculation

A simulation of the temperature field was made for the imposed geometry of the roll but with no regard to convection in the liquid.

It was assumed that convection did not have a huge effect on a temperature value estimated for the midpoint located between two walls of the mould and at its given height.

Commercial Finite Element Software ABAQUS was used for simulation of a temperature field behaviour in function of time. The temperature field resulting from the *Green-Naghdi* basic energy balance and the *Fourier* law was considered:

$$\int_V \rho \dot{U} dV = \int_S q dS + \int_V \sigma dV \tag{1}$$

$$f = -\lambda \frac{\partial T}{\partial z} \tag{2}$$

with assumed boundary conditions shown in Fig. 1.

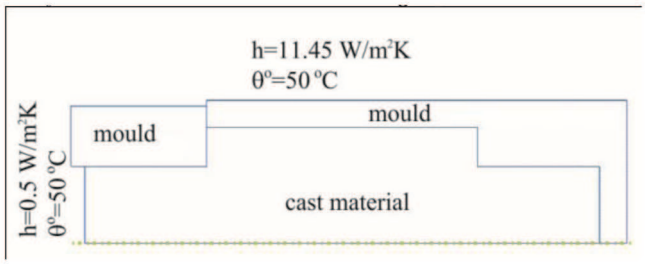

Fig. 1. Geometry of the system and its boundary conditions

3. Operating point for the C→E transition

It was postulated that the midpoint in the ceramic mould (middle of the ceramic mould thickness), set at the middle of the roll length, is the representative place for temperature field observation, and especially for the $C \rightarrow E$ transition, Fig. 2. This place was named the operating point of the temperature field for the solidifying roll. In fact, changes of temperature versus time at the operating point forms a plateau, Fig. 2.

The plateau is situated between $t_C \leftrightarrow t_E$ for the applied ceramic mould, shown in Fig. 2. The estimated values of both parameters are as follows: $t_C \approx 5.9$[h] and $t_E \approx 7.9$[h].

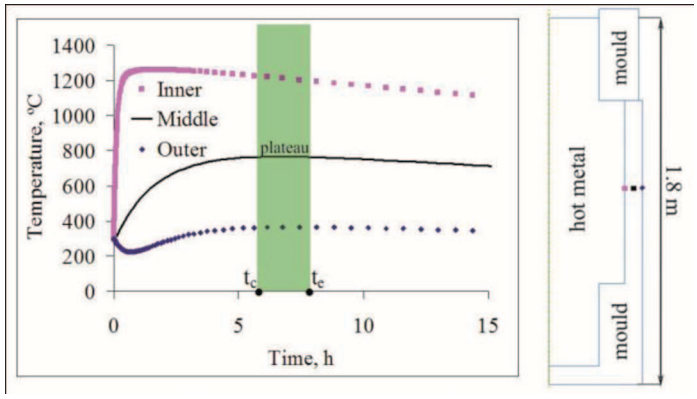

Fig. 2. Temperature versus time behaviour for the ceramic mould; *Inner* – point situated at the contact: roll surface/ceramic mould, *Outer* – point situated at the ceramic mould surface (air contact), *Middle* – midpoint of the ceramic mould (half the mould thickness); calculations performed for solidification of a cast steel roll

The behaviour of the temperature field created at the operating point situated at the half the thickness of the mould (operating point was defined in Fig. 2) is shown schematically in Fig. 3.

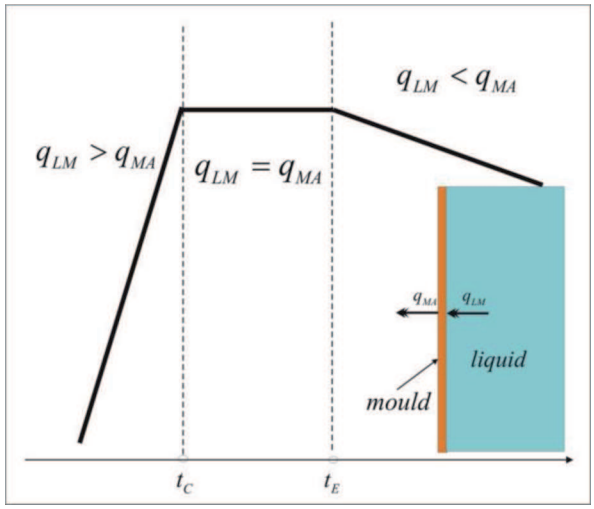

Fig. 3. Changes of temperature in function of time at the operating point situated in the middle of the ceramic mould; a/$\dot{T} \gg 0$, for $t < t_C$, b/$\dot{T} = 0$, for $t_C < t < t_E$, c/$\dot{T} < 0$, for $t > t_E$; q_{LM} – heat flux from the liquid into the mould; q_{MA} – heat flux from the mould into the air

The tmperature field calculated for solidification of the cast steel roll is shown in Fig. 4. The *liquidus* temperature is equal to 1363 [^{0}C] and *solidus* temperature is equal to 1131 [^{0}C].

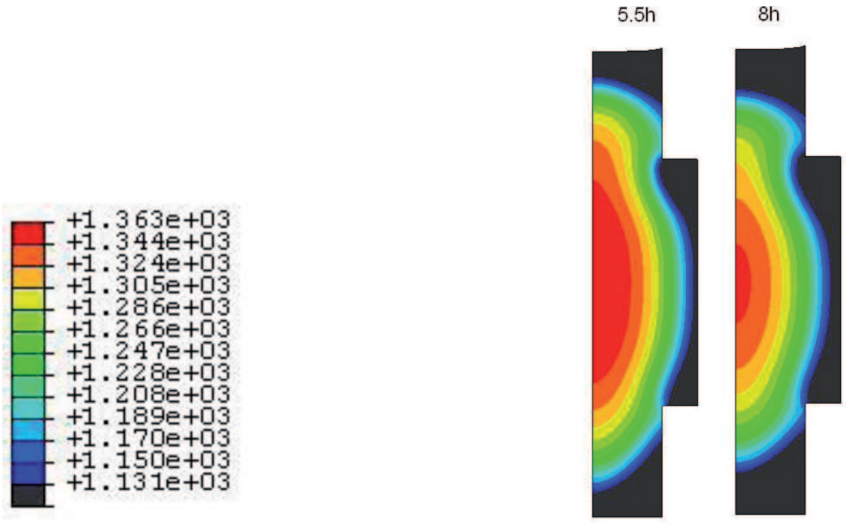

Fig. 4. Temperature field calculated for solidification of the cast steel roll and shown just before – time and slightly after the – time

The *solidus* isotherm is reproduced by the *navy blue/black* boundary. It is visible that *solidus* isotherm was shifted during period of time denoted $t_C \leftrightarrow t_E$.

It means that an amount of precipitates located in between the columnar grains increased.

However, the *liquidus* isotherm touched the symmetry axis of the roll even at the time t_C.

It can be concluded that *liquidus* isotherm is no more in the contact with columnar dendrites/cells tip, beginning at $t + t_C^R$. The *liquidus* isotherm goes through the liquid to make the liquid temperature lower than the equilibrium liquidus temperature and to stimulate the equiaxed structure growth.

The temperature field for the cast iron roll mould is shown in Fig. 5.

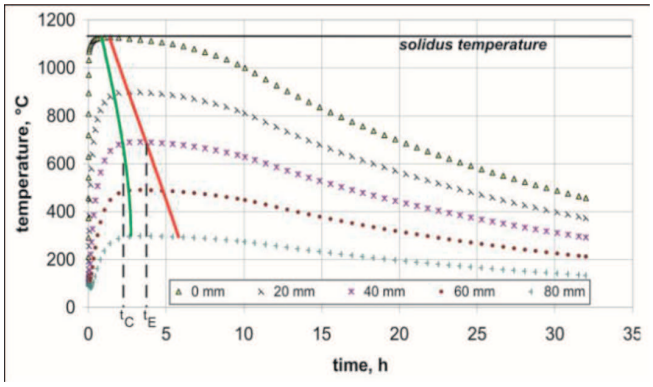

Fig. 5. Changes of temperature in function of time at different points situated in the ceramic mould as calculated for a cast iron roll

The difference $t_C^R - t_C$ denotes the delay between appearance of the operating point plateau and an actual commencement of the columnar structure vanishing.

Intersection of vertical curves with temperature profile printed for the midpoint of the mould (denoted: ×40 [mm]) defines the period of time denoted $t_C \leftrightarrow t_E$, Fig. 5.

The analyzed plateau appeared significantly smaller in the case of the cast iron roll solidification, Fig. 5, when compared with the analogous plateau delimited for the cast steel roll solidification, Fig. 2.

4. Analysis of the temperature field for the cast iron roll solidification

The $C \rightarrow E$ transition from the columnar structure formation into the fully equiaxed structure formation for the solidification of the cast iron roll manifests itself in the ceramic mould at the period of time defined as follows: $t_C \approx 2.6$[h]; $t_E \approx 3.8$[h], Fig. 5. The temperature field considered before and just after that time are shown in Figs 6-9.

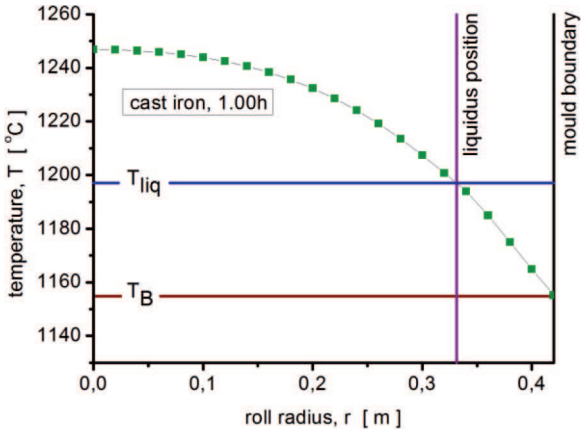

Fig. 6. Temperature field calculated for the time equal to 1.0 [h] within the cast iron roll of the 950 [mm] in diameter

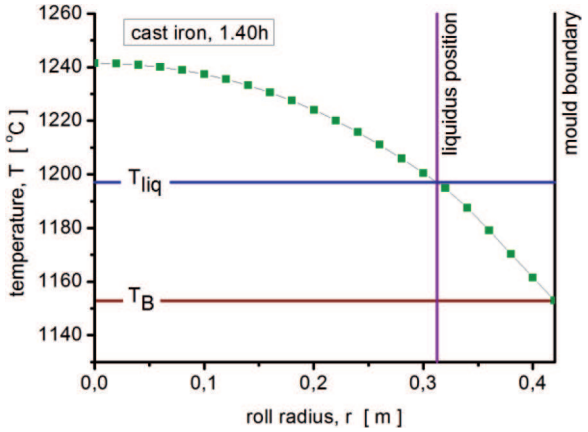

Fig. 7. Temperature field calculated for the time equal to 1.4 [h] within the cast iron roll of the 950 [mm] in diameter

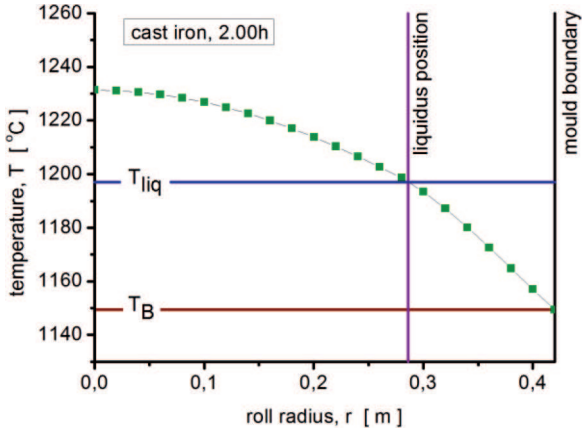

Fig. 8. Temperature field calculated for the time equal to 2.0 [h] within the cast iron roll of the 950 [mm] in diameter

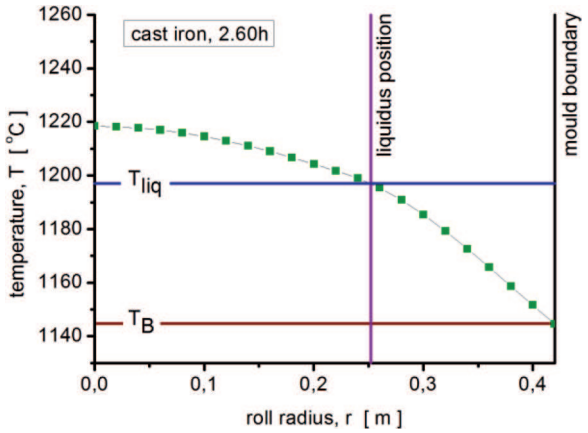

Fig. 9. Temperature field calculated for the time equal to 2.6 [h] within the cast iron roll of the 950 [mm] in diameter

The results of simulation shown in Figs 6-9 allowed to develop the graph that presents the movement of the *liquidus* isotherm, that is a velocity of the *liquidus* isotherm in function of time for the whole solidification process under investigation, Fig. 10.

It is evident that the movement of the *liquidus* isotherm is inseparably connected to the solid phase formation.

Additionally, the rate of temperature changes observed at the inner surface of the mould are also presented, to compare it with the rate of the *liquidus* isotherm movement, Fig. 10.

Both curves were expected to be similar. A distinct similarity is visible. Yet, a certain delay between the curves also occurred.

The $t_C^R \leftrightarrow t_E^R$ period of time was marked on the basis of the *liquidus* isotherm movement analysis presented in Fig. 10. According to the analysis, it should be emphasized that *liquidus* isotherm velocity decreases within period of time $t < t_C^R$, when columnar structure growth is expected.

It means that columnar growth slows down and finally the *liquidus* isotherm velocity manifests its minimum.

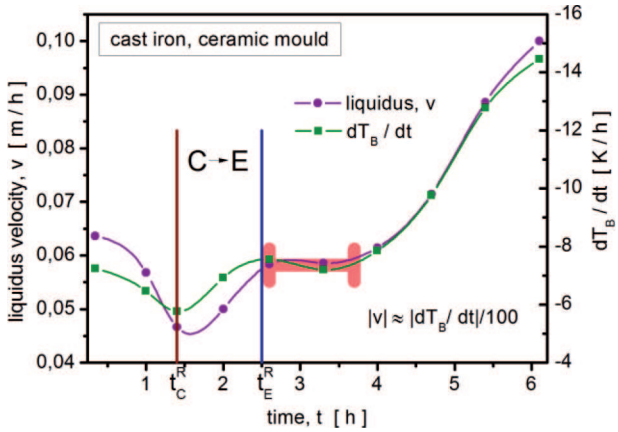

Fig. 10. Velocity of the *liquidus* isotherm movement in function of time; additionally dT_B/dt, as observed at the roll/mould border is shown; the $t_C^R \leftrightarrow t_E^R$ period of time is distinguished

The competition between columnar and equiaxed structure formation starts before the minimum when the *liquidus* isotherm accelerates. It is assumed that the *liquidus* isotherm tears away from the columnar dendrite/cell tips at time $t = t_C^R$. Therefore, the t_C^R – time is situated at the first flexibility point of the v – curve and at the minimum of the $\dot{T}_B$ – curve, simultaneously. Columnar structure is still formed within the period of time $t_C^R \leftrightarrow t_E^R$, but its growth vanishes due to the lost competition, and at the time $t = t_E^R$ the equiaxed structure growth dominates, exclusively. The t_E^R – time is located at the second flexibility point of the v – curve.

Additionally, similarity between the analyzed curves is visible, and a certain delay between both curves, between minima, Fig. 10.

The delay in time is justified, because a sequence of the envisaged phenomena occurs in the air/mould/ingot system.

First, the q_{MA} – heat flux appears as a result of the q_{LM} – heat flux existence, and next a movement of the *liquidus* isotherm is expected in the sequence. The discussed delay vanishes at about the fourth hour of solidification, when the last and a very large portion of the liquid becomes undercooled in the whole volume. This phenomenon involves the presence of the nucleation within the whole remaining volume of the liquid.

5. Analysis of the thermal gradients field

Not only the analysis of temperature field but also the analysis of the thermal gradients field is possible. The thermal gradients behaviour observed at the columnar dendrite/cell tips allowed to differentiate the zone of the columnar structure formation from the zone of the fully equiaxed structure formation, [1]. However, the mentioned analysis, [1] is based on the calculation of the solid/liquid interface undercooling only. The current calculation of the temperature field allows to show the thermal gradients field without taking into account the undercooling, Figs. 11-13. It is an advantage of the current mode of calculation. According to the current model,

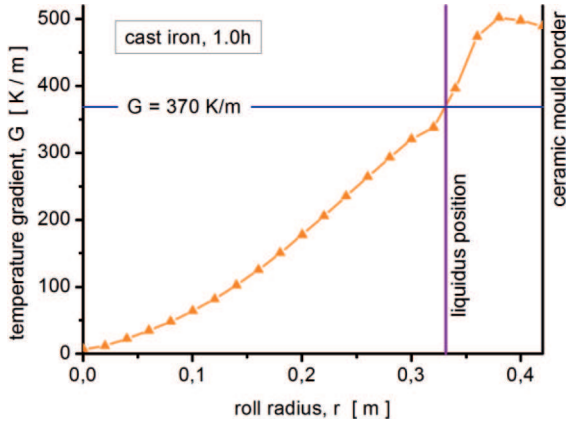

Fig. 11. Thermal gradients field calculated for time: 1.0 [h]; estimation of the thermal gradient value at the s/l interface

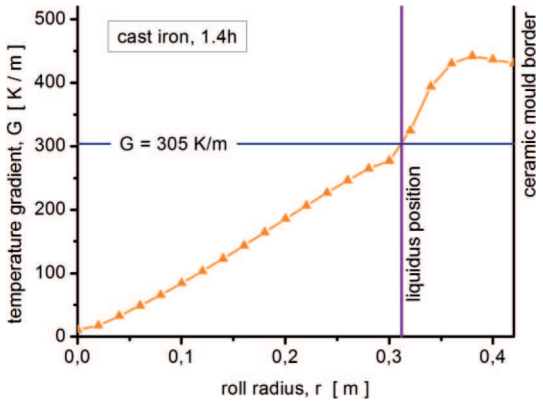

Fig. 12. Thermal gradients field calculated for time: 1.4 [h]; estimation of the thermal gradient value at the s/l interface

determination of the temperature field, rate of the liquidus isotherm movement and thermal gradients field by means of numerical treatment is sufficient to localize $C \rightarrow E$ transition within solidification time and along the roll radius.

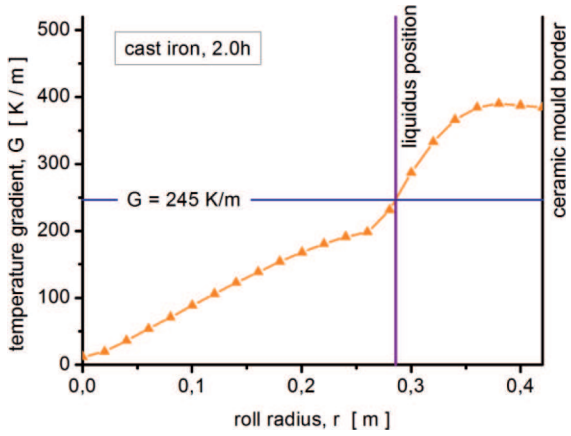

Fig. 13. Thermal gradients field calculated for time: 2.0 [h]; estimation of the thermal gradient value at the s/l interface

The results shown in Figs 11-13 allow to present changes of thermal gradients in function of time, Fig. 14.

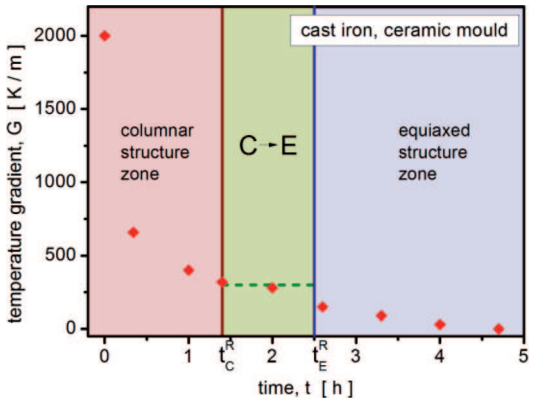

Fig. 14. Changes of the thermal gradient during solidification; changes are observed at the solid/liquid interface: first, at the tips of columnar dendrites/cells, next on the solid/liquid interface of a layer of the equiaxed grains (deposited on the surface of columnar structure layer due to thermophoresis and gravity phenomena); the $t_C^R \leftrightarrow t_E^R$ period of time representing the $C \rightarrow E$ transition is taken from Fig. 10 and superposed

It can also be explained how the vanishing of columnar structure occurs in time. It is assumed that at the beginning of the columnar structure zone formation the velocity of growth is equal to the velocity of the *liquidus* isotherm movement. Starting from the t_C^R time an extrapolation of the columnar growth velocity to its zero value should be marked, Fig. 15.

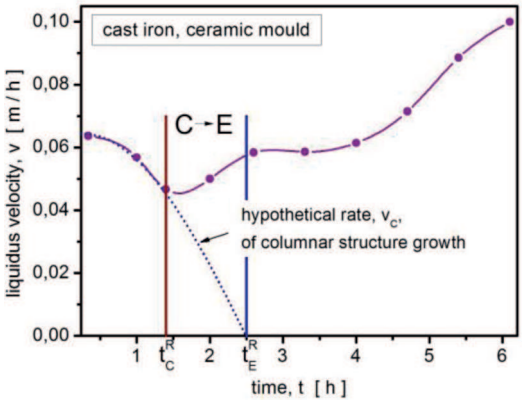

Fig. 15. Extrapolation of the columnar growth velocity to determine the time, t_E^R, that defines a full vanishing of the columnar structure

The extrapolation of the columnar growth velocity to its zero value shows that columnar structure formation is no longer possible starting from time denoted t_E^R, and defined in Fig. 10.

At that time, competition between columnar structure and equiaxed structure is completed and fully equiaxed structure can be formed exclusively.

6. Solute redistribution in solidifying rolls

Not only thermal gradients field can be associated with the different structure formation (columnar or equiaxed), Fig. 14, but the solute redistribution can be also referred to direct observations of the structure. A measurement of solutes redistribution within the cast iron roll solidified in the semi-industry conditions was made, Figs. 16-17.

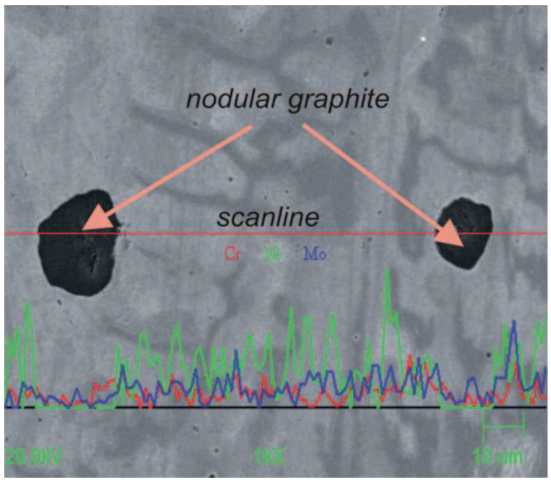

Fig. 16. Morphology of the cast iron roll revealed at 3 [mm] from the roll surface; black particles – nodular graphite, dark areas – cementite, bright areas – austenite; small particles of the graphite are also visible

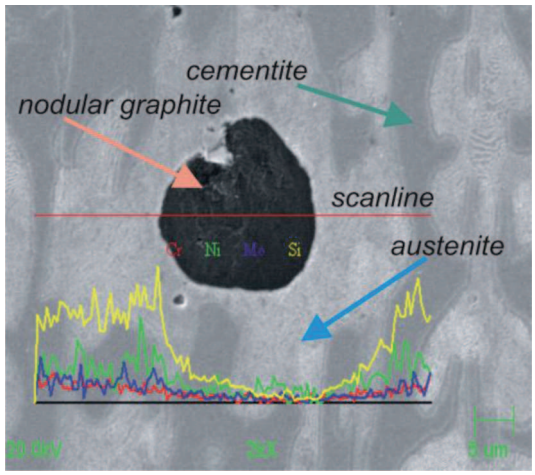

Fig. 17. Morphology of the eutectic grain in the cast iron roll (nodular graphite enveloped by austenite); small particles of nodular graphite situated inside the austenite are also visible

The recent model, [6], for the prediction of the solute redistribution allows to confront the measured profile of redistribution within the primary phase with the adequate theoretical profile.

The amount of an eutectic precipitate accompanying the primary phase can also be predicted theoretically, [6]. The primary phase which is observable in solidifying roll is austenite, Figs 18-19. Some carbides are situated at the boundary of the columnar grains of austenite or inside the austenite grains, Fig. 18.

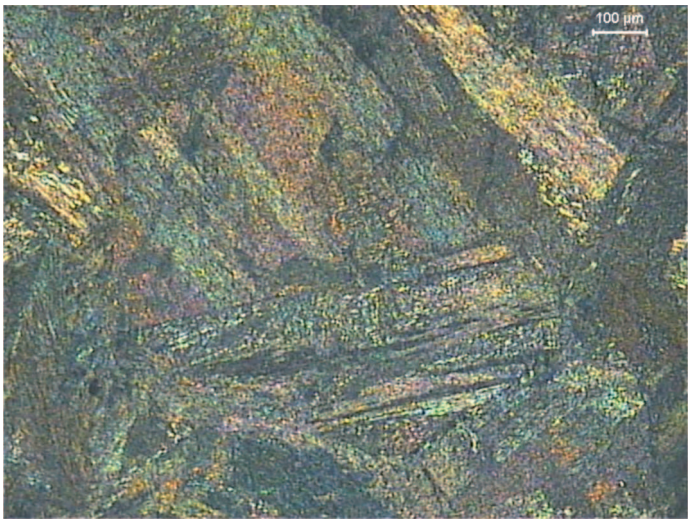

Fig. 18. Columnar structure of the austenite revealed in the cast steel roll just at its surface; primary phase (austenite) contains small particles of carbides; some carbides are also situated at the boundary of austenite grains, [13]

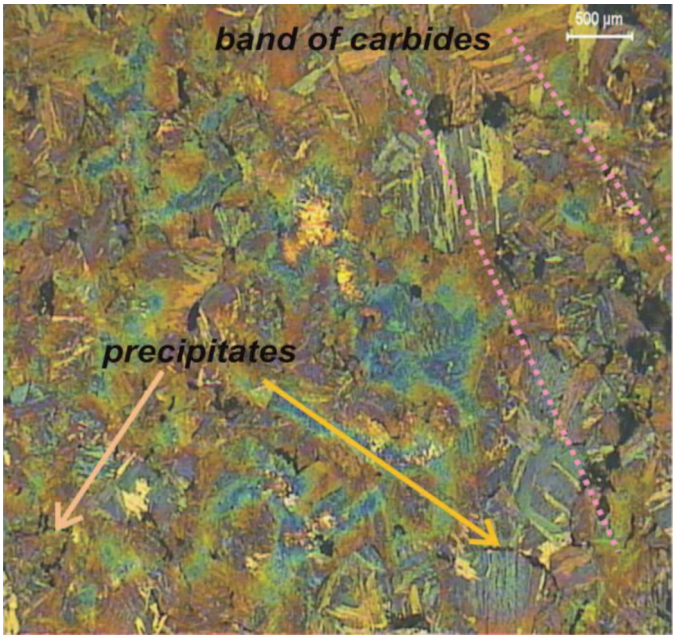

Fig. 19. Equiaxed structure revealed in the cast steel roll just at its axis; primary phase (austenite) is surrounded by precipitates resulting from the microsegregation phenomenon; a band containing large carbides resulting from the macrosegregation is also visible, [13]

More information about the solute redistribution within the columnar structure can be obtained from the experiment made on the laboratory scale, in the *Bridgman* furnace, Fig. 20. However, the system should be equipped with an auxiliary allowing the solidification to be arrested and morphology to be frozen, Fig. 20.

In this case the solid/liquid interface can be revealed, which allows studying its geometry.

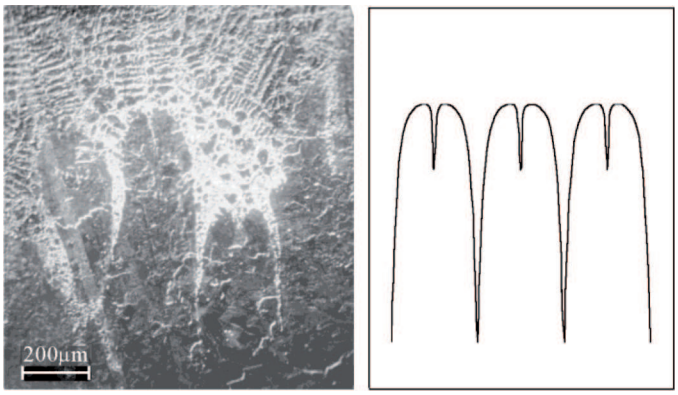

Fig. 20. Morphology of the columnar cells: a) as frozen due to the solidification arrested at a given time and occurring in the steady-state conditions; b) as reproduced theoretically; tips splitting are also: a) revealed, and b) reproduced theoretically, [12]

An equiaxed structure can be easily obtained on the laboratory scale by means of common solidification process, Fig. 21. This structure can also be frozen to allow observation of the solid/liquid interface geometry. Measurement of the solute redistribution is more accurate when solidification is completed, Fig. 21.

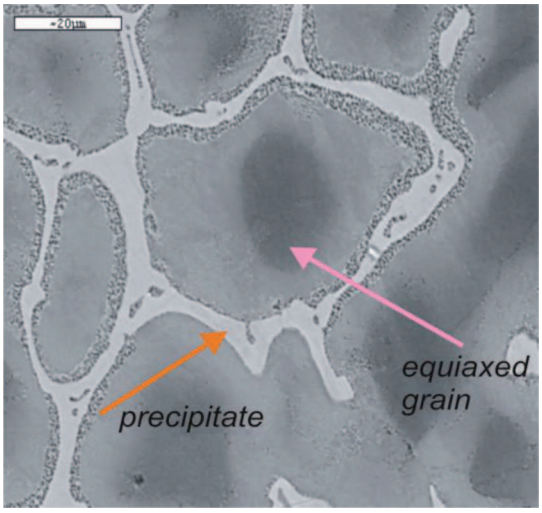

Fig. 21. Typical equiaxed structure containing a primary phase surrounded by a precipitate, [8]

The following equation is proposed to describe a solute redistribution after back-diffusion, (with α defined in [7]):

$$N_B\left(x,x^0,\alpha\right)=\left[k+\beta^{ex}\left(x,x^0\right)\beta^{in}\left(x^0,\alpha\right)\right]N_L\left(x,\alpha\right) \quad (3)$$

This equation is universal and can be used to study the solute redistribution within: a/ the columnar structure (2D analysis), Fig. 20, and b/ the equiaxed structure (3D analysis), Fig. 21.

In the case of columnar structure four modes of solute redistribution measurement are suggested, Fig. 22:

a/ at the bottom of a frozen columnar grain:

$$N_B\left(x,1,\alpha\right)=\left[k+\beta^{ex}\left(x,1\right)\beta^{in}\left(1,\alpha\right)\right]N_L\left(x,\alpha\right) \quad (4a)$$

b/ at a certain height of a frozen columnar grain:

$$N_B\left(x,x^0\left(\bar{L}_0\right),\alpha\right)= \left[k+\beta^{ex}\left(x,x^0\left(\bar{L}_0\right)\right)\beta^{in}\left(x^0\left(\bar{L}_0\right),\alpha\right)\right]N_L\left(x,\alpha\right) \quad (4b)$$

c/ along the axis of symmetry of a frozen columnar grain:

$$N_B\left(0,x^0,\alpha\right)=\left[k+\beta^{ex}\left(0,x^0\right)\beta^{in}\left(x^0,\alpha\right)\right]N_L\left(0,\alpha\right) \quad (4c)$$

d/ along the envelope of a frozen columnar grain:

$$N_B\left(x^0,x^0,\alpha\right)=\left[k+\beta^{ex}\left(x^0,x^0\right)\beta^{in}\left(x^0,\alpha\right)\right]N_L\left(x^0,\alpha\right) \quad (4d)$$

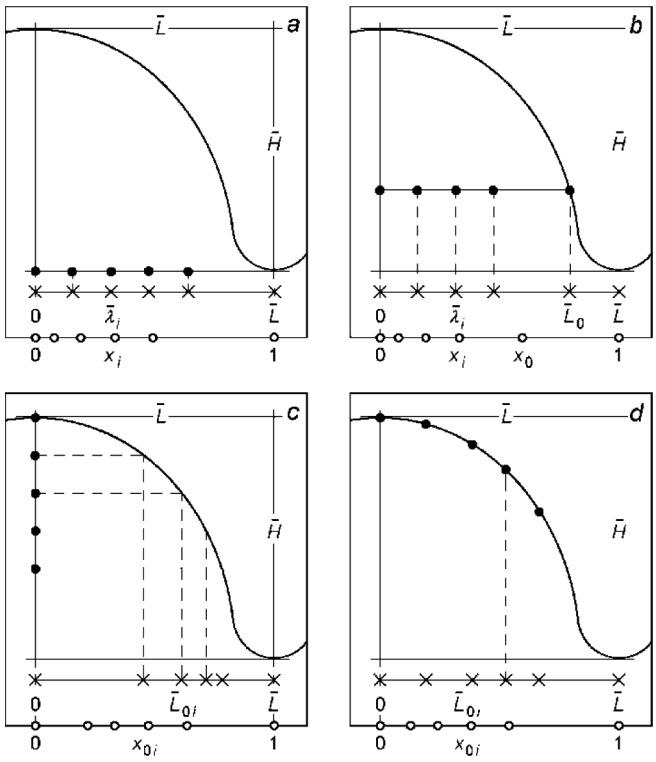

Fig. 22. Rules of the solute redistribution measurement for the frozen columnar structure; black dots are the measurement points, [6]

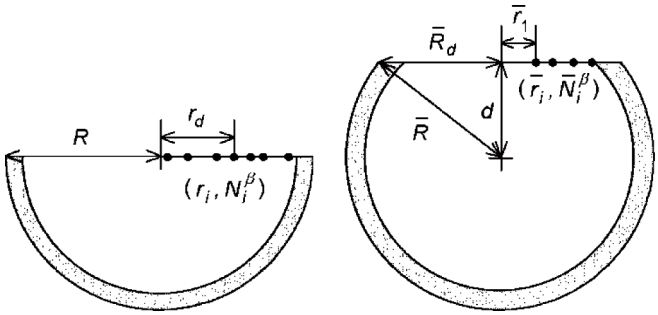

Fig. 23. Rules of the solute redistribution measurement for the equiaxed structure; black dots are the measurement points, [8]; left scheme shows the main intersection of the representative equiaxed grain; right scheme shows the lateral intersection of a given equiaxed grain; coordinates of points located on the surface of lateral intersection should be displaced concentrically onto the surface of the main intersection, (for example: a point on lateral intersection which has $\bar{r}_1$ – coordinate after displacement onto main intersection has r_d – coordinate)

In the case of the equiaxed structure, the following mode of solute redistribution measurement is suggested, Fig. 23:

a/ for the main intersection of the equiaxed grain,

$$N_B\left(x\left(r_i\right),1,\alpha\right) = \left[k+\beta^{ex}\left(x\left(r_i\right),1\right)\beta^{in}\left(1,\alpha\right)\right]N_L\left(x\left(r_i\right),\alpha\right) \tag{5}$$

b/ for the lateral intersection of the equiaxed grain the above equation can be used once again under condition, however, that the coordinates of measurement points are displaced from the lateral intersection into the main intersection.

The method of displacement is explained in detail in Fig. 23.

The displacement requires to determine the d – parameter that is the distance between the lateral intersection and the main intersection.

The major difficulty is to determine the distance between the lateral intersection and the main intersection.

For that reason some additional solutions can be applied such as: inserting of the visible nucleus in the centre of an equiaxed grain, [8], or its successive polishing.

The successive polishing allows to observe the behaviour of the perimeter of the analyzed intersection of the equiaxed grain. The larger the perimeter becomes the more the d – distance reaches zero.

The eutectic precipitate was analyzed by the EDAX technique. The solute redistribution profile was revealed for both phases: austenite and cementite. One example of measurement associated with the manganese redistribution across the lamellae is shown in Fig. 24.

An average redistribution is also suggested (red line). The resultant profile (red line) can be described theoretically using a relationship between the concentration micro-filed in the liquid and some parameters taken from the phase diagram together with some capillary parameters, [9]. The solution to diffusion equation resulting in the concentration micro-filed for the liquid is attainable, [10], [14].

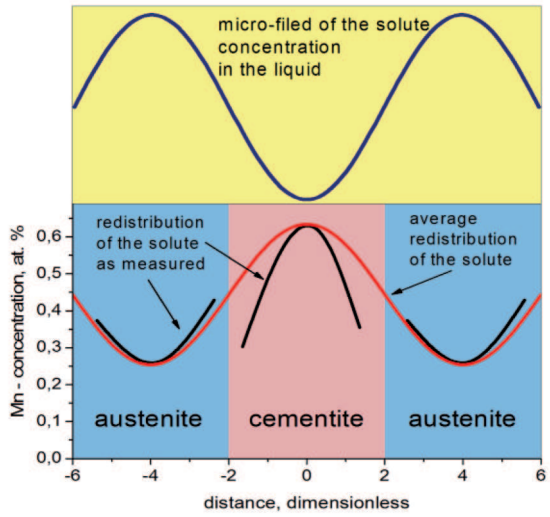

Fig. 24. Mn – solute redistribution across the eutectic lamellae

7. Concluding remarks

The proposed method of the localization of the $C \rightarrow E$ transition requires neither arduous measurement nor experiment, as it is suggested in the literature, [3].

It is sufficient to know some material parameters which are easily accessible.

The parameters are easily accessible even in the case of industrial situation.

Moreover, the theoretical predictions could be verified to some extent by the temperature measurement: a/ at the operating point, b/ at the roll / mould border (T_B – temperature).

A difference between localization in time of the $t_C \leftrightarrow t_E$ period and the $t_C^R \leftrightarrow t_E^R$ incubation period is established.

The $t_C^R - t_C$ difference equals -1.2[h], with the $t_C \approx 2.6$[h], Fig. 5, and with the $t_C^R \approx 1.4$[h], Fig. 10, Fig. 15. The $t_E^R - t_E$ difference is equal to -1.3[h], with the $t_E \approx 3.8$[h], Fig. 5, and with the $t_E^R \approx 2.5$[h], Fig. 10, Fig. 15.

The $t_C \leftrightarrow t_E$ period of time (plateau in Fig. 5) corresponds well with the period of time: $2.6[h] \leftrightarrow 3.7[h]$, (bar in Fig. 10) for which the curve dT_E/dt evinces an expected flatness.

The stationary state of the heat transfer evinces itself during the $t_C \leftrightarrow t_E$ period of time, Fig. 2, Fig. 3, Fig. 5, Fig. 14.

It can be justified by the identity: $q_{LM} \approx q_{MA}$, Fig. 5.

Since the abatement of the T_B – temperature to some extent corresponds to the movement of the *liquidus* isotherm, Fig. 10, it is justified to measure some changes of the T_B – temperature during the industrial foundry processes.

A differentiation between velocity of the columnar structure tips and velocity of the *liquidus* isotherm, Fig. 15, defines the time t_C^R.

An independent relationship which shows the interplay between velocity of columnar structure tips and tips radius at a given temperature gradient observed at the tip is known, [11].

This analytical relationship allows to determine the velocity of the columnar structure growth and to compare it with the one resulting from the analysis shown in Fig. 15.

It could be very useful in a more specific determination of the t_C^R – time.

It should be said that the differentiation, Fig. 15, occurs when the thickness of the solid layer is large enough to convert the activity of the solid more as an isolator than as a conductor.

The *solidus* isotherm appears when first precipitates are present between columnar dendrites/cells and the fully developed mushy zone is observed within the solidifying roll.

It is concluded that only the midpoint in the mould is neutral for heat transfer (no influence of air and no influence of the liquid cast iron/cast steel).

Thus, the midpoint can be representative in determining the $t_C \leftrightarrow t_E$ period of time as it was assumed.

Three ranges within the thermal gradient field determined for the solidifying roll were distinguished:

a/ for the formation of the columnar structure (the C – zone):

$\dot{T} \gg 0$, Fig. 5, and $\left(G\Big|_{t<t_C^R} - G\Big|_{t=t_C^R}\right) \gg 0)$, Fig. 14,

b/ for the $t_C \leftrightarrow t_E$ transition (from columnar to fully equiaxed structure): $\dot{T} \approx 0$, Fig. 5, and $\left(G\Big|_{t=t_C^R} - G\Big|_{t=t_C^R}\right) \approx 0$, Fig. 14,

c/ for the formation of the fully equiaxed structure (the E – zone): $\dot{T} < 0$, Fig. 5, and $\left(G\Big|_{t=t_C^R} - G\Big|_{t>t_C^R}\right) \approx 0$, Fig. 14.

The b/ – range can be referred directly to the analysis based on the undercooling calculation that results in determination of the G_{crit}, (1).

According to mentioned analysis, [1], there are:

a/ high thermal gradients for the columnar structure formation; the thermal gradients should be higher than their critical value, G_{crit},

b/ low thermal gradients for the equiaxed structure formation; the thermal gradients should be lower than above critical value, G_{crit}.

The current model of the behaviour of thermal gradients, Fig. 14, is similar to that based on the undercooling calculation.

There are some difficulties and uncertainties how the high thermal gradients and low thermal gradients together with the critical thermal gradient could be precisely determined, [1].

The current model shows the mode of determination of the thermal gradient – time diagram, Fig. 14, together with Fig. 10, Fig. 15, according to which an accurate value of the $t_C^R \leftrightarrow t_E^R$ period of time is the result of the numerical treatment of the heat transfer.

This type of calculation can be applied directly even in the industrial conditions.

Hypothetical time, t_E^R, of the complete vanishing of columnar structure formation, Fig. 10, was confirmed with a good agreement through the extrapolation explained in Fig. 15.

The measurement of the solute segregation can be applied subsequently to the calculations associated with the analysis of a temperature field behaviour together with thermal gradient field behaviour.

This analysis based on:

a/ the solute redistribution measurement within the columnar structure,

b/ the solute redistribution measurement in the equiaxed structure,

c/ the determination of the precipitation amount,

can reveal a difference between both redistributions in the micro-scale.

Moreover, this comparison can give some explanations of the origins of the segregation/ redistribution as observed in the macro-scale.

Thus, determination of the macrosegregation maps is possible.

The macrosegregation can be described by a macrosegregation index defined as follows:

$$i_{macr.} = \left[N_B^{\max} - N_B^{\min}\right]/N_0 \tag{6}$$

Both the redistribution analysis and the macrosegregation analysis employ the α – back diffusion parameter defined in (7). The physical meaning imposed for this parameter, [6] allows the practical use of the parameter in some simulations associated with the mass transfer.

It should be stated that its value tends to unity for solidifying massive rolls.

Acknowledgements

The financial support from the Polish Ministry of Science and Higher Education (MNiSW) under contract N R15 006 004 is gratefully acknowledged.

The assistance of the "Huta Buczek – Sosnowiec, Poland" - Rolls Foundry is greatly appreciated.

REFERENCES

[1] J.D. Hunt, Steady State Columnar and Equiaxed Growth of Dendrites and Eutectics, Materials Science and Engineering **65**, 75-83 (1984).

[2] A.E. Ares, C.E. Schvezov, Solidification Parameters during Columnar-to-Equiaxed Transition in Lead-Tin Alloys, Metallurgical and Materials Transactions **31A**, 1611-1625 (2000).

[3] M. Hamdi, M. Bobadilla, H. Combeau, G. Lesoult, in: Modelling of Casting, Welding and Advanced Solidification Processes VIII, eds B.G. Thomas and Ch. Beckerman. TMS, 375-382 Warrendale, PA, 1998.

[4] Ch.A. Gandin, From Constrained to Unconstrained Growth during Directional Solidification, Acta Materialia **48**, 2483-2501 (2000).

[5] ABAQUS Theory Manual,Academic Computer Centre CYFRONET, AGH – University of Science and Technology.

[6] W. Wołczyński, Back-Diffusion Phenomenon during the Crystal Growth by the Bridgman Method, Chapter 2. in the book: Modelling of Transport Phenomena in Crystal Growth, eds J.S. Szmyd and K. Suzuki, WIT Press, 19-59 Southampton – Boston, 2000.

[7] H.D. Brody, M.C. Flemings, Solute Redistribution in Dendritic Solidification, AIME Transactions **236**, 615-623 (1966).

[8] W. Wołczyński, W. Krajewski, R. Ebner, J. Kloch, The Use of Equilibrium Phase Diagram for the Calculation of Non-Equilibrium Precipitates in Dendritic Solidification. Theory, Calphad **25**, 401-408 (2002).

[9] G. Lesoult, M. Turpin, Etude Theorique sur la Croissance des Eutectiques Lamellaires,Memoires Scientifiques de la Revue de Metallurgie **66**, 619-631 (1969).

[10] W. Wołczyński, Concentration Micro-Field for Lamellar Eutectic Growth, Defect and Diffusion Forum **272**, 123-138 (2007).

[11] W. Wołczyński, R. Martynowski, J. Kowalski, W. Wajda, Langer & Muller-Krumbhaar Criterion in the Description of the Liquid Concentration at a Growing Dendrite Tip, Chapter: Ma-

terial Processing in: Proceedings of the 7^{th} World Conference on Experimental Heat Transfer, Fluid Mechanics and Thermodynamics, eds J.S. Szmyd, J. Spałek, T.A. Kowalewski, 1913-1920 Kraków – 2009.

[12] M. Faryna, W. Wołczyński, T. Okane, Micro-analytical Techniques Applied to Phase Identification and Measurement of Solute Redistribution at the Solid/Liquid Interface of Frozen Fe-4.3Ni Doublets,Mikrochimica Acta **139**, 61-65 (2002).

[13] W. Wołczyński, E. Guzik, W. Wajda, B. Kania, Columnar ==> Equiaxed Structure Transition in Solidifying Rolls, Proceedings of the 14 International Heat Transfer Conference – IHTC14, Washington – 2010, Melting and Solidification, p. 9.1-9.10 IHTC14-23048.

[14] W. Wołczyński, J. Kloch, Mass Transport at the Solid/Liquid Interface during in situ Growth of Composites, Archives of Metallurgy and Materials **49**, 339-354 (2004).

Received: 10 April 2011.